Journal of Membrane Science 595 (2020) 117526

Contents lists available at ScienceDirect

Journal of Membrane Science

journal homepage: http://www.elsevier.com/locate/memsci

Few-layers MoS_2 nanosheets modified thin film composite nanofiltration membranes with improved separation performance

Shishi Yang [a,b], Kaisong Zhang [a,*]

[a] Key Laboratory of Urban Pollutant Conversion, Institute of Urban Environment, Chinese Academy of Sciences, Xiamen, 361021, PR China
[b] University of Chinese Academy of Sciences, Beijing, 100049, PR China

ARTICLE INFO

Keywords:
MoS_2
Thin film nanocomposite
Nanofiltration membrane
Interfacial polymerization
"Trade-off" phenomenon

ABSTRACT

Two-dimensional (2D) molybdenum disulfide (MoS_2) nanosheets materials with excellent properties provide a new possibility and approach for designing nanofiltration (NF) membranes with overcoming the "trade-off" phenomenon of permselectivity. Few-layers of 2D MoS_2 were synthesized by a facile solvent-assisted ultrasonic exfoliation method. A novel nanocomposite NF membrane was fabricated through interfacial polymerization by addition of the as-prepared MoS_2 nanosheets into the organic phase at different concentrations. The characterization of field-emission scanning electron microscope (FE-SEM) and transmission electron microscope (TEM) confirmed that MoS_2 nanosheets were successfully embedded in the membranes. As a result, the hydrophilicity, electronegativity and cross-linking degree of the membranes were significantly enhanced. The membrane achieved its best performance at a MoS_2 concentration of 0.010 wt/v% with about 2.3 times increment in water permeability without sacrificing salt rejection compared to the control membrane. Moreover, the modified membrane exhibited higher stability over a long-term test. This provides new thinking and guidance for the industrial preparation of NF with excellent separation performance.

1. Introduction

Membrane technology as an effective water purification method to solve water pollution and water limitation has attracted wide attention [1]. Nanofiltration (NF) membrane has been recognized because of its advantages of low operating pressure and inexpensive equipment maintenance cost [2–5]. However, the conventional thin film composite (TFC) membrane is limited by the "trade-off" phenomenon in the permselectivity [6–10]. Therefore, it is vital to prepare the novel NF membrane with high permeability without sacrificing selectivity.

Recently, many researchers have devoted on improving the separation performance of TFC membrane by incorporating the two-dimensional (2D) nanomaterials into the selective polyamide (PA) layer to prepare thin film nanocomposite (TFN) membrane [11–13]. By taking the advantages of their atomic thickness, hydrophilicity, antibacterial property, surface charge characteristics as well as their ease of preparation, the resulted TFN membranes are expected to out-performed the-state-of-art of commercial membranes and existed polymeric TFC membranes [14]. Graphene oxide (GO) is one of the hottest 2D nanomaterials studied in recent years as a result of its excellent hydrophilicity properties [6,15–22]. However, the GO membrane is unstable in an aqueous environment due to the presence of a large amount of oxygenated functional groups, and is easy to swell [23]. The researchers attempt to improve the swelling phenomenon and enhance its stability through the thermal treatment reduction of GO, while inevitably reduced the original layer spacing of GO and greatly sacrificed the permeability of pure water [24]. This method increases economic costs but not achieving the expected results. Furthermore researchers found that the new 2D material hexagonal boron nitride (h-BN) has good hydrophilicity and mechanical stability, and is expected to improve the permeability of the membrane [25–28]. However, during the research of modified h-BN, it was found that the resulting membrane did not show adequate selectivity properties [29,30].

Novel molybdenum disulfide (MoS_2) based on superior properties (such as excellent mechanical properties, electronegativity, hydrophilicity and fouling resistance) has been found promising in the field of membrane technology [11,31–39]. MoS_2 displays smooth surface without any oxygenated functional groups, reducing the resistance of water molecules to transport [37]. Molecular dynamics simulation proves that MoS_2 with pore structure has superior separation performance and the flux obtained from MoS_2 membrane was 3–5 times more compared to GO when prepared under the same conditions [40–42].

* Corresponding author.
E-mail address: kszhang@iue.ac.cn (K. Zhang).

https://doi.org/10.1016/j.memsci.2019.117526
Received 10 July 2019; Received in revised form 26 September 2019; Accepted 29 September 2019
Available online 7 October 2019

Experimental conditions, such as phase inversion, pressure-assisted assembly, layer-by-layer self-assembly and other methods, have shown enhanced hydrophilicity and antifouling performance, while they are incorporated after the complex modification of pure MoS_2. This undoubtedly increases the economic cost. More importantly, it has great difficulties in the field of desalination [31,43–45]. In our earlier work [11], we found that TFN reverse osmosis (RO) membrane showed a dramatic improvement in separation performance due to the negatively charged 2D MoS_2 nanosheets, which was responsible for the salt ions repulsion of the enhanced membrane surface. Besides, the increased hydrophilic site of exfoliated nanosheets gave rise to a more hydrophilic membrane surface. This successfully confirmed that the introduction of MoS_2 into the membrane could simultaneously increase the water flux and salt rejection. Based on the successful research of RO membrane, we hypothesize that MoS_2 can also play a role in NF, since the NF membrane is a separation process by pore size and charge effect, the charge plays a crucial role. Changing the amount of charge on the membrane can effectively improve the rejection of the divalent salt, and increased hydrophilicity is expected to enhance the permeation flux. Based on those work, we anticipated that the advanced 2D MoS_2 nanosheets could endow the TFC membrane with enhanced separation performance by tailoring the membrane surface physicochemical characteristics through incorporating MoS_2 nanosheets in the PA layer.

Compared to the chemical method that requires the use of inflammable and explosive chemicals, the liquid exfoliation was considered to be safer and more reliable due to its simplicity, environmental friendliness, low cost and high productivity [46–49]. In this work, we improved the previous high-energy exfoliation method for MoS_2 [11], few-layers of MoS_2 nanosheets were prepared with a much lower power (500 w) input and less exfoliation time (12 h) consumed using KQ-500DE. The hydrophilic, negatively charged MoS_2 nanosheets was added to the organic phase to prepare NF membrane by interfacial polymerization on the polysulfone (PSf) ultrafiltration (UF). The crystal structure, chemical property and charge property of MoS_2 were characterized. The effects of the MoS_2 nanosheets on NF membrane surface morphology, membrane structure and the physicochemical properties were systematically investigated. The stability and the hydraulic resistance of the fabricated TFN membrane were evaluated in a long-term filtration using the saline water. The separation performance test of the membrane showed that the modified membrane can simultaneously improve permeability and selectivity. It is expected to realize its industrial scale application at a lower cost, and provide a theoretical reference for the design and preparation of low-pressure NF membranes in the future.

2. Experiment

2.1. Materials

The PSf UF membrane was prepared in the laboratory through phase inversion method and used as a support layer of NF for subsequent experiments. The aqueous phase monomer was piperazine (PIP, 99%), organic phase monomer was 1,3,5-benzenetricarbonyl trichloride (TMC, 98%), acid absorber was triethylamine (TEA, 99%), (±)-Camphor-10-sulfonic acid (CSA, 99%) was used to adjust pH, the four inorganic salts Na_2SO_4 (99%), $MgSO_4$, $MgCl_2$ (99.9%) and NaCl (99.5%) which used in the separation performance test and electrolyte solution KCl (99.99%) in the zeta potential test were purchased from Aladdin. 1-Methyl-2-pyrrolidinone (NMP), surfactant sodium dodecyl sulfate (SDS), polyethylene glycol (PEG) and *n*-hexane was the solvent for TMC were supplied by Sinopharm Chemical Reagent Co., Ltd. Molybdenum disulfide (MoS_2) was supplied from Sigma-Alorich. All the water involved in this experiment was deionized (DI) water.

2.2. Preparation of MoS_2 nanosheets

Similar to the previous work, MoS_2 with few-layers was obtained by solvent-assisted exfoliation of commercially available bulk MoS_2 [11]. Briefly, 1.0 g of MoS_2 powder was immersed in 200 mL of NMP solution and placed in a KQ-500DE ultrasonic machine for several hours with 500 w to obtain uniform dispersion solution. During the whole ultrasonic process, ice packs were used to keep the ultrasonic temperature of the water bath below 30 °C, so as to avoid the evaporation of NMP organic solvent caused by the overheating. The solution was centrifuged in Centrifuge 5430R at 2000 rpm for 20 min, and was collected and filtered under 0.22 μm poly tetra fluoroethylene (PTFE) microfiltration membrane, the deposits were repeatedly washed with DI water to remove residual NMP, finally dried in an oven at 60 °C for about 48 h.

2.3. Fabrication of MoS_2 NF membrane

Phase inversion technique was used for the fabrication of the PSf UF base membrane [50]. The casting solution was applied to the nonwoven fabric at a knife height of 200 μm and speed at 4 m/s, while the UF membrane pure water flux was 220 $L\,m^{-2}\,h^{-1}$ and the bovine serum albumin (BSA) rejection of 98.1% was tested by a dead-end filter cell at 1.0 bar. The PSf UF membranes were stored in 0.5% sodium bisulfite solution ($NaHSO_3$) to prevent contamination.

Before interfacial polymerization, PSf UF membrane was soaked in DI water to remove $NaHSO_3$ solution remaining on the surface. Rinsed the membrane with plenty of DI water and dried at ambient temperature. Firstly, the aqueous solution containing 92.28 wt% DI water, 3.00 wt% CSA, 3.00 wt% TEA, 0.12 wt% SDS and 1.60 wt% PIP were deposited onto the surface of the PSf UF membrane for 45 s, residual PIP aqueous solution was absorbed in 3 min with tissue papers. Followed immersed in 0.35 wt/v% TMC dissolved in *n*-hexane organic phase containing different amount (0.000, 0.004, 0.008, 0.010, 0.012 and 0.014 wt/v%) of MoS_2 for 20 s. After that, the membrane was dried in an oven at 60 °C for 2 min, and finally stored in DI water for later use. In order to facilitate the subsequent expression, we named the content of prepared MoS_2 at 0.000, 0.004, 0.008, 0.010, 0.012 and 0.014 wt/v% as M0, M1, M2, M3, M4 and M5, respectively.

2.4. Characterization of MoS_2

The effect of different ultrasonic time on MoS_2 was observed by field-emission scanning electron microscope (FE-SEM, S-4800, HITACHI, Japan). MoS_2 powder and the prepared crystals lamellar structures were characterized by transmission electron microscope (TEM, Talos-S, FEI, USA) under the operating voltage of 200 kV. The thickness of the exfoliated MoS_2 was examined by atomic force microscopy (AFM, Dimension Icon, Bruker, USA) to observe the number of layers. The crystal structure and the d-spacing of MoS_2 were revealed by X-ray diffraction (XRD, X'Pert Pro, PANalytical, Netherlands). The charge of MoS_2 was analyzed by zeta potential (Zeta PALS, Malvern, Britain), the MoS_2 was dispersed in DI water to form solutions at pH values ranging from 3 to 10. The binding energy of Mo 3d and S 2p of MoS_2 were revealed by X-ray photoelectron spectroscopy (XPS, ESCALAB 250XI, Thermo, USA).

2.5. Characterization of MoS_2 NF membrane

Before characterization, all the membranes were dried in the oven at 60 °C for at least 48 h. The effects of 2D nanomaterials on the surface and cross-section morphology of the TFC and TFN membranes were observed by field-emission scanning electron microscope (FE-SEM, S-4800, HITACHI, Japan) and transmission electron microscope (TEM, H-7650, HITACHI, Japan). The surface roughness of membranes with the incorporation of MoS_2 was examined by atomic force microscopy (AFM, Dimension Icon, Bruker, USA). The membrane was dropped with 5 μl DI water and evaluated the hydrophilicity by contact angle analyzer

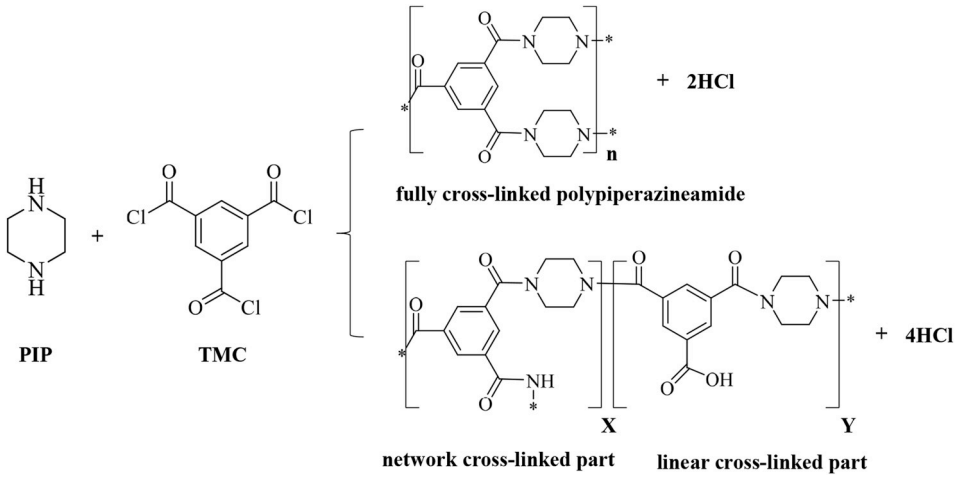

Fig. 1. Interfacial reaction of PIP with TMC to form cross-linked NF membrane.

(DSA100, KRUSS, German). The surface charge of the membranes was tested by zeta potential (SurPASS 3, Anton Paar, Australia) with 1 mM KCl electrolyte solution, the pH was adjusted by the 0.05 mol/L HCl and NaOH, the gap height was about 100 μm. The atomic composition of M0-M5 was determined by X-ray photoelectron spectroscopy (XPS, Axis Supra, Kratos, Britain). The molecular weight cut-off (MWCO) of NF membranes was characterized by TOC-Vcph analyzer (Shimadzu, Japan).

2.6. Density and cross-linking degree of NF membrane

The density of the membrane was related to the cross-linking degree of the membrane and could be measured from the XPS test of the membrane surface [51], the reaction equation of PIP and TMC was shown in Fig. 1. The ratio of O and N could be obtained by the XPS test, and the corresponding degree of network cross-linking (DNC) was calculated according to Eqs. (1) and (2).

$$\frac{O}{N}=\frac{3X+4Y}{3X+2Y} \tag{1}$$

$$DNC(\%)=\frac{X}{X+Y}\times 100 \tag{2}$$

where X and Y represent the network cross-linked structure and the linear cross-linked structure, respectively.

2.7. Pore size and pore size distribution of NF membrane

In general, MWCO for NF membranes was tested using 1000 ppm of different molecular weights PEG (200–1000 Da), the rejection was calculated in the same way as the salt. When the rejection was 90%, the corresponding molecular weight was the MWCO of the membrane, and the 50% rejection was the corresponding mean effective pore diameter (μ_p) of the membrane. According to the following Eqs. (3)–(5), the pore size and pore size distribution could be analyzed [52,53].

$$a=16.73\times 10^{-10}\times M_{PEG}^{0.557} \tag{3}$$

$$d_s=2\times a\times 10^{7} \tag{4}$$

$$\frac{dR(d_p)}{dd_p}=\frac{1}{d_p ln\sigma_p\sqrt{2\pi}}exp\left[-\frac{\left(lnd_p-ln\mu_p\right)^2}{2\left(ln\sigma_p\right)^2}\right] \tag{5}$$

where a (cm) and d_s (nm) represent the Stokes radius and diameter of the solute PEG at the corresponding MWCO, respectively. Under the

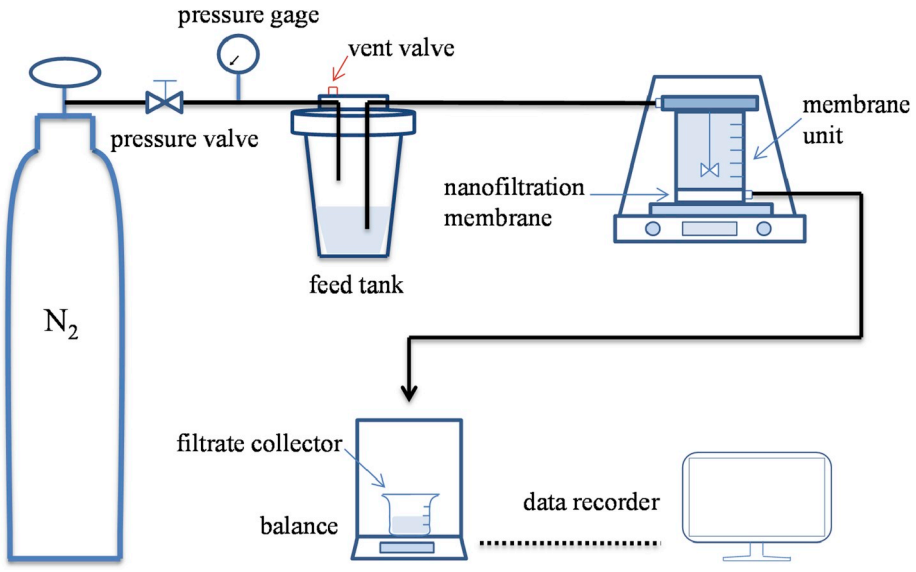

Fig. 2. The test mechanism of the prepared NF membranes separation performance.

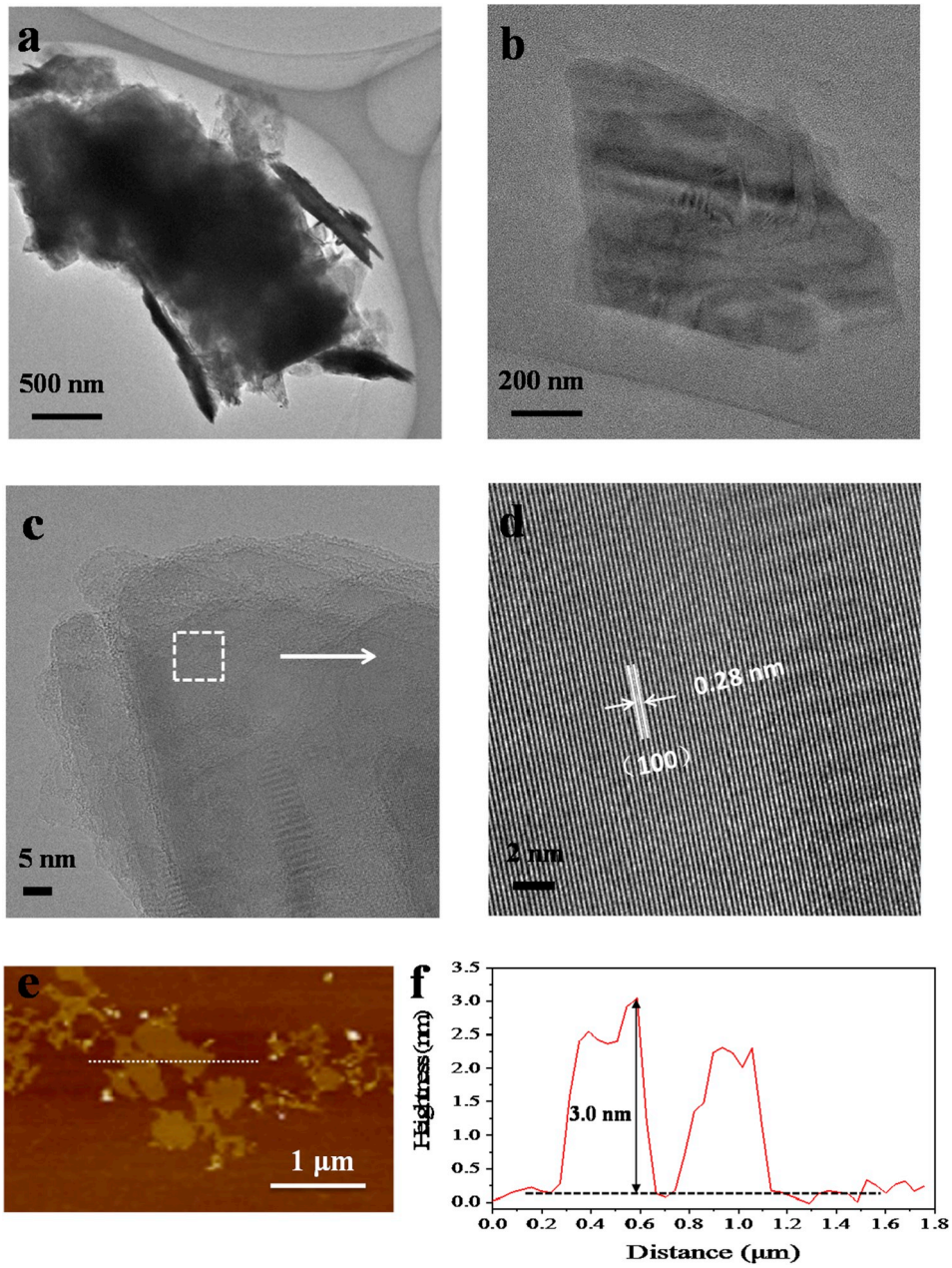

Fig. 3. TEM of MoS_2 0 h (a) and MoS_2 12 h (b–d) and AFM of exfoliated MoS_2 (e–f).

condition of ignoring the hydrodynamic and electrostatic interactions between the solute PEG and the pores of the membrane, the Stokes diameter (μ_s) at PEG rejection of 50% is defined as the mean effective pore diameter (μ_p) of the membrane. The ratio of the Stokes diameter when the PEG rejection is 84.13% and 50% is defined as the geometric standard deviation (σ_g), which is approximately equal to the geometric standard deviation (σ_p).

2.8. Desalination performance of MoS_2 NF membrane

The desalination performance of the NF membranes was examined by a lab-scale dead-end filter cell, the experiment scheme was illustrated in Fig. 2. The operating procedure was as follows: the nitrogen of 3.5 bar was used to pressurize the feed tank, feed solutions were performed at 2000 ppm and were pressed to the membrane unit, the magnetic stirring speed was controlled at 350 rpm to avoid deposition contamination. The mass of the permeation was counted by the balance, and finally saved in the computer. Each one of the membranes was prepress for 30 min before starting the test and the separation performance was evaluated according to the following formula.

The water flux of the permeable solution was measured by Eq. (6):

$$J_w = \frac{Q}{At} \tag{6}$$

where J_W is the permeation flux (L m^{-2} h^{-1}), Q is the total volume of permeate water (L) for the duration of time t (h), and A is the testing area of the membrane (m^2).

During the whole test process, the permeate solutions were collected after the membrane was prepressed for 30 min, conductivity meter (sensION + EC5, HACH) was used to measure the conductivity. Since the conductivity was related to the concentration, the separation performance was calculated by Eq. (7):

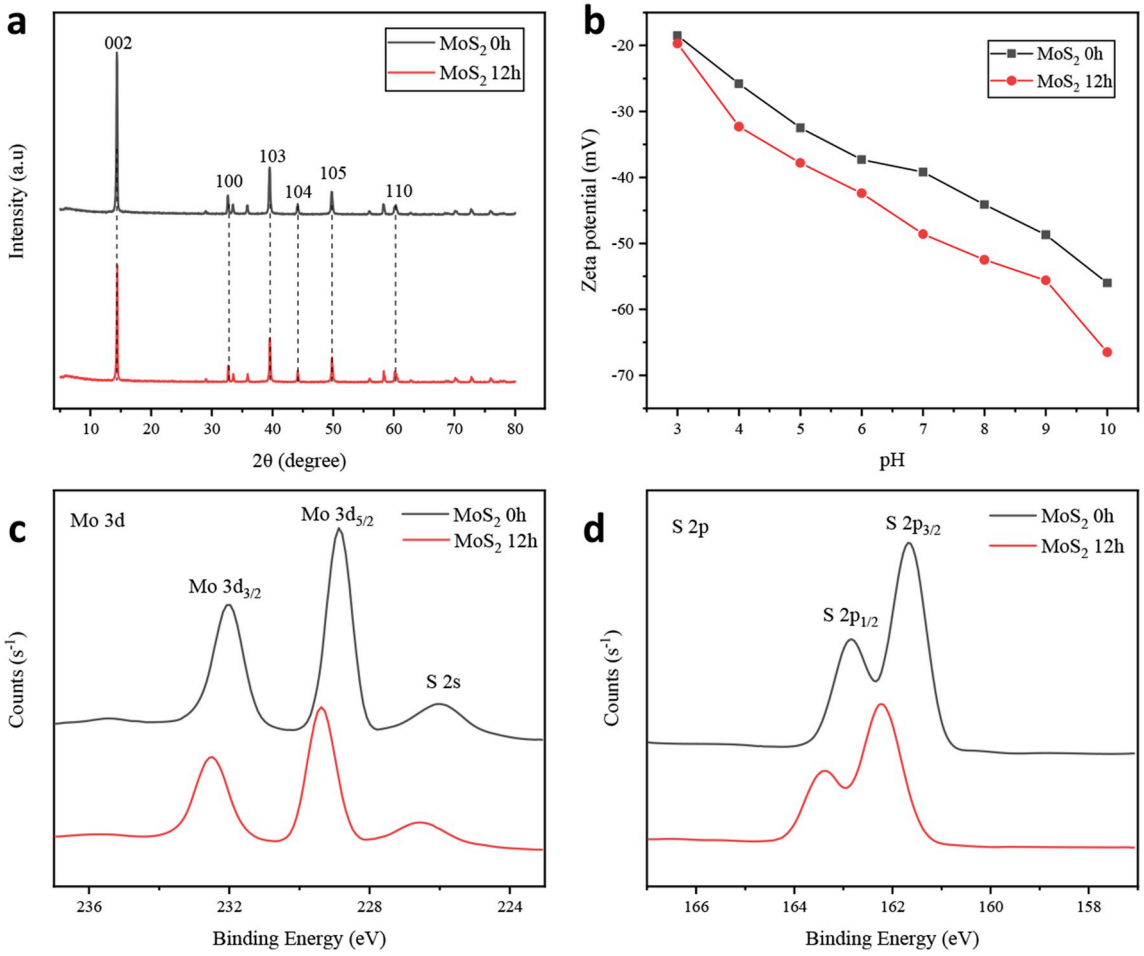

Fig. 4. XRD (a), zeta potential (b), high-resolution XPS spectra of (c) Mo 3d and (d) S 2p for bulk MoS_2 and the prepared MoS_2.

$$R(\%) = \left(1 - \frac{C_p}{C_f}\right) \times 100 \quad (7)$$

where C_p and C_f are the salt concentration of permeate and feed solutions, respectively.

3. Results and discussion

3.1. Determine the optimal ultrasound time

This work first discussed the influence of ultrasonic time on MoS_2 nanomaterials and even on the properties of membranes. The effects on the layers structure and lateral size of MoS_2 nanosheets were observed 30,000 times using scanning electron microscope (SEM) magnification as shown in Fig. S1. It could be found in Fig. S1(a) that the original MoS_2 powder layer was thicker and the lateral dimension was larger. With the further increment in ultrasonic time, the nanosheets tended to shatter and fall off, especially to 12 h [46]. Considering the economic cost caused by the long ultrasound time, we initially considered 12 h as the better ultrasound time.

Fig. S2 revealed the results of the separation performance of the prepared MoS_2-TFN with MoS_2 0.010 wt/v% at different ultrasonic time. It was further determined that the MoS_2-TFN membrane permeability and selectivity were optimal when the ultrasonic time was 12 h. As the ultrasonic time prolonged, the size of the prepared MoS_2 nanosheets gradually decreased. The nanosheets with larger size were more ready to distribute horizontally in the selective matrix, while smaller nanosheets were prone to distribute randomly in the PA layer [54]. The nanosheets with smaller size are failed to construct the water channels, the non-selective voids created by the spaces among nanosheets and the voids between nanosheets and polyamide matrix may provide the extra salt passages. At the same time, the defects resulted from the agglomeration of nanosheets could deteriorate the salt rejection [55].

For the preparation of NF membranes by adding MoS_2 in the organic phase, there are two advantages. Firstly, adding nanoparticles directly into the organic phase by taking the advantage of the good volatilization property of *n*-hexane, which did not require drying, the charged MoS_2 nanosheets materials could be directly distributed on the surface of the membrane after drainage the organic phase, which closer to the surface of the separation layer was expected to protect the PA layer [56]. Besides, the incorporated MoS_2 could be maximum their functionalities (2D size, hydrophilicity and negative charge) when those nanosheets distributed on membrane surface [57].

3.2. Physicochemical characterization of MoS_2

The original bulk MoS_2 and the exfoliated MoS_2 (12 h) were further observed by transmission electron microscope (TEM). As represented in Fig. 3a, the bulk MoS_2 displayed a multi-layer structure. The lateral size of exfoliated MoS_2 layers in Fig. 3b was significantly reduced. The layer structure was confirmed by the high-resolution transmission electron microscope (HRTEM) in Fig. 3c-d. By randomly selecting different positions and averaging, the lattice spacing was about 0.28 nm, corresponding to (100) plane. The morphology and thickness of the exfoliated MoS_2 were observed by atomic force microscopy (AFM) and shown in Fig. 3e-f. Since the gap between the adjacent two layers of MoS_2 was about 0.62 nm [58], the prepared MoS_2 had a structure within 5 layers.

The characteristic peaks were characterized by X-ray diffraction

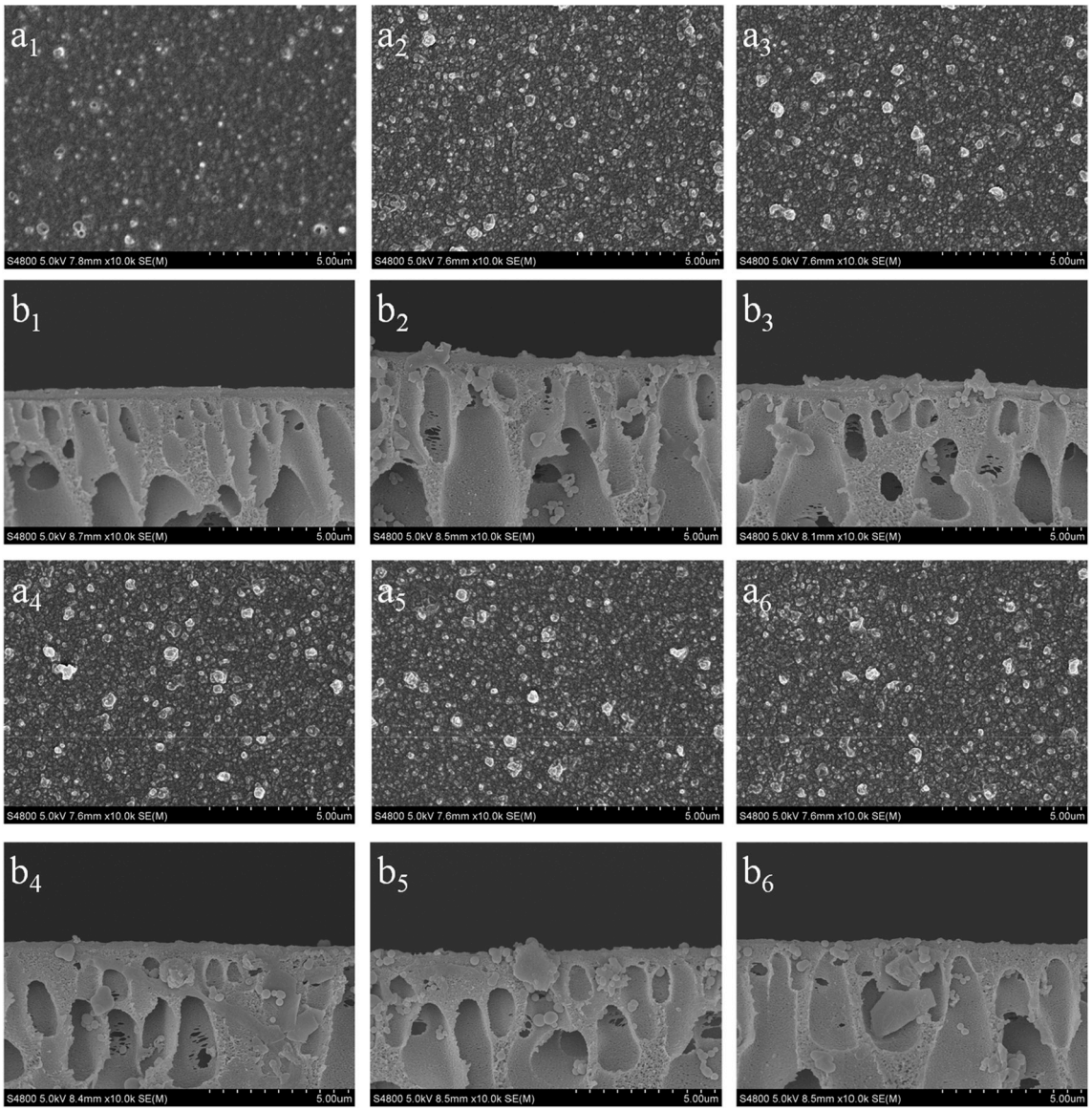

Fig. 5. SEM surface (a_1-a_6) and cross-section (b_1-b_6) morphologies of M0-M5 NF membranes.

(XRD) as described in Fig. 4a. The strong peak at $2\theta = 14.3^\circ$ was corresponding to the (002) plane, and the layer spacing was about 0.62 nm according to the Bragg's law $n\lambda = 2d\sin\theta$, which was consistent to the literature [11]. Zeta potential was utilized to analyze the charged property of nanomaterials, Fig. 4b showed that both the bulk MoS_2 and the prepared MoS_2 showed a high negative charge in a wide pH range. The zeta potential of the exfoliated MoS_2 nanosheets was as low as −48.6 mV when the pH was 7. Due to the energy input during the exfoliation process, the edge of the MoS_2 nanosheets could be destroyed inevitably, which giving rise to the exposure of sulfur (S) atoms along with the edge of the nanosheets [11]. The chemical structure of the MoS_2 was analyzed by X-ray photoelectron spectroscopy (XPS). The results (Fig. 4c-d) were consistent to other report [59]. It could be obviously observed that the Mo peak and the S peak were migrated to the high energy region due to the decrease of the electron cloud density after ultrasonic process [60].

3.3. Characterization of MoS_2 NF membranes

SEM was used to observe the surface and cross-section morphologies of NF membranes. In Fig. 5a_1-a_6, the membranes exhibited a typical bubble structure because of the fast reaction between PIP and TMC [61]. The MoS_2 was uniformly distributed on the surface of the TFN membrane without significant agglomeration. Similarly, in Fig. 5b_1-b_6, MoS_2 was also distributed in the PA layer without producing defects. TFC (M0) and TFN (M3) membranes were selected to observe the cross-section structure by TEM. As shown in Fig. 6, as the inorganic nanoparticles exhibited a black random structure under the TEM electron beam, this signified that the prepared MoS_2 nanosheets were successfully incorporated in the PA layer. Combined with the result from the SEM, it could be concluded that MoS_2 was successfully embedded on the membrane surface as well as in the PA matrix.

The three-dimensional (3D) scan (10 μm × 10 μm) image of AFM was used to observe the effect of the MoS_2 incorporation on the membrane surface roughness, as shown in Fig. 7. The membranes exhibited an increased surface roughness due to the incorporation of the MoS_2 nanosheets compared to the pristine membrane. The surface roughness parameters (average roughness: Ra, root mean-square roughness: Rq, maximum vertical distance: Rz) were summarized in Table 1.

Fig. 8a-b illustrated that with the addition of MoS_2, the electronegativity and hydrophilicity of the MoS_2-TFN membranes were significantly improved. Under the neutral condition, the zeta potential of the

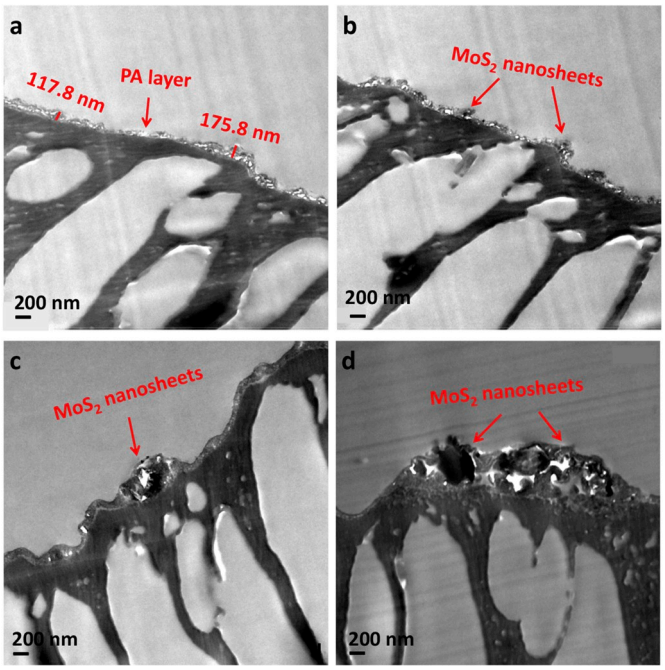

Fig. 6. TEM cross-section morphologies of M0 (a) and M3 (b–d) membranes.

membrane increased up to −32.8 mV at 0.010 wt/v% of MoS_2, this could be related to the strong electronegativity of MoS_2. According to the literature [62], the contact angle of MoS_2 was about 70°. Adding the MoS_2 to the TFC membrane could change the contact angle of the MoS_2-TFN membrane from 84.7° to 51.4°, and the increasing in hydrophilicity had a great influence in enhancing the membrane flux. According to the data of DNC (%) presented in Table 2, the selective layer of membrane became denser, which might be due to the addition of MoS_2 to form a Mo–O covalent bond (~531 eV) that promoted the further formation of the amide (~532 eV) during the interfacial polymerization. Consequently, reducing the amount of carboxylic acids (~533.5 eV) formed by the final hydrolyzed of unreacted acyl chloride in Fig. 8c-d [12,60].

3.4. Filtration performance of MoS_2 NF membranes

As shown in Fig. 9a-b, the molecular weight cut-off (MWCO) of the TFN membrane (373 Da) was reduced compared to the TFC membrane (507 Da) after the incorporation of MoS_2. In the calculation done, when PEG retention rate was 50%, the μ_p of TFC and TFN membrane was 0.64 and 0.57 nm, respectively. This improvement was consistent with the further enhanced of the cross-linking degree of the membrane after modification as shown in Table 2. The pure water flux of the TFN membrane was greatly improved with increasing MoS_2 under the test pressure of 3.5 bar as shown in Fig. 9c. At the addition of 0.010 wt/v% MoS_2, the pure water flux enhanced from 12.1 L m^{-2} h^{-1} (3.4 L m^{-2} h^{-1} bar^{-1}) to 27.1 L m^{-2} h^{-1} (7.8 L m^{-2} h^{-1} bar^{-1}), which was 2.3 times higher than the pristine TFC membrane. In Fig. 9d, as the operating

Table 1
Surface roughness parameters of membranes with different loading concentration of MoS_2:Ra, Rq, Rz.

Membrane NO.	Ra (nm)	Rq (nm)	Rz (nm)
M0	16.2	22.0	267
M1	17.2	26.8	332
M2	18.4	28.4	410
M3	20.9	30.4	430
M4	22.8	32.7	400
M5	23.0	38.4	549

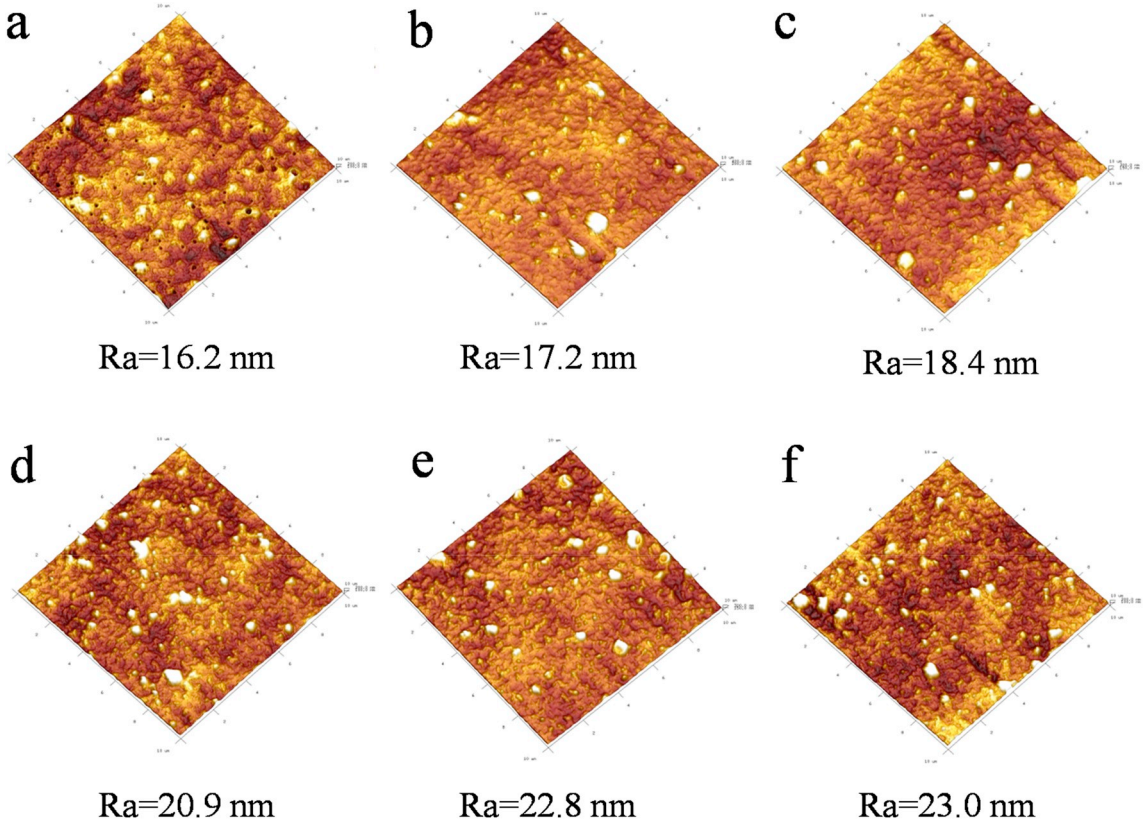

Fig. 7. AFM 3D morphologies of M0-M5 NF membranes.

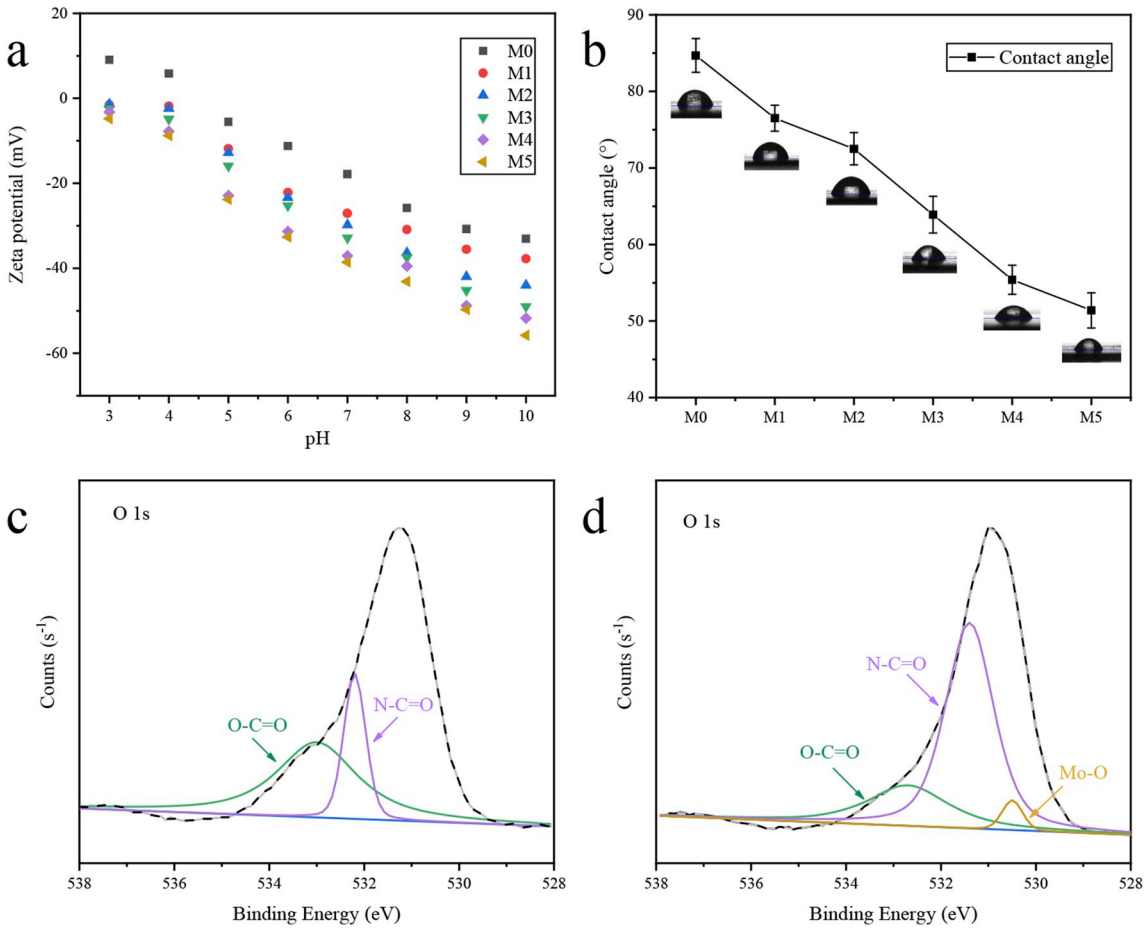

Fig. 8. Zeta potential (a) and contact angle (b) of membranes with different adding concentration and XPS core level spectra of O1s for M0 (c) and M3 (d).

Table 2
Degree of cross-linking of TFC and MoS_2-TFN membranes.

Membranes	C	N	O	S	Mo	O/N	DNC (%)
M0	85.30	5.70	9.00	–	–	1.58	32.83
M1	82.82	7.05	10.01	0.09	0.03	1.42	47.58
M2	78.02	9.34	12.46	0.14	0.04	1.33	57.15
M3	76.40	10.40	12.99	0.15	0.06	1.25	67.01
M4	75.19	10.98	13.61	0.15	0.07	1.24	67.86
M5	73.96	11.71	14.07	0.16	0.10	1.20	72.45

pressure increased from 2.5 bar to 5.0 bar, the pure water flux of the membrane at the concentration of 0.010 wt/v% presented a linear upward trend, which would greatly help the future application of the membrane in various fields. The salt permeation and rejection of TFN membranes with MoS_2 added to the organic phase at different concentrations vary greatly. As shown in Fig. 9e, the rejection of the four salts was improved in the M3 membrane. Combined with Fig. 9c, it could be concluded that the loading of 2D nanosheets MoS_2 greatly enhanced the desalination performance of the TFN membranes, which optimal concentration was determined to be 0.010 wt/v%. A significant improvement could be observed in Fig. 9f when comparing the control M0 with M3 membrane in pure water flux and the permeation of the four salts.

The improvement in pure water flux was attributed to 1) Increased hydrophilicity of MoS_2-TFN membranes, which could be attributed to the hydrophilic sites on the MoS_2 nanosheets could form hydrogen bonds with water molecules, thus accelerating the transportation of water molecules [11,63]. 2) The surface roughness was slightly increased, as reported in the literature, a rougher surface provided more contact area for water molecules [64,65]. The increase in salt rejection could be attributed to 1) The size sieving effect resulted from the enhanced degree of cross-linking of the selective layer [66,67]. 2) The improved surface zeta potential also had a positive effect in separation of multi-valent salt ions because of the Donnan effect. In general, the rejection sequence of the four salts was as follows: $Na_2SO_4 > MgSO_4 > MgCl_2 > NaCl$, which was consistent with the many negatively charged NF membranes [68–70].

In Table 3, the separation performance of the TFC membrane and MoS_2-TFN membrane were compared with other recently reported MoS_2 membranes. It was observed that the MoS_2-TFN membrane prepared in this experiment showed a greatly improved flux, and the desalination performance was significantly improved in contrast with other membranes. This indicated that the MoS_2-TFN membrane was undoubtedly a very significant breakthrough and expected to achieve its own good value in the field of water treatment in the future. Table S1 also compared the desalination performance with some typical commercial NF membranes [71], the flux of TFN membrane prepared in this work exceeded that of many NF membranes with the same selectivity performance, which was competent to the commercial NF membranes in water desalination.

3.5. *Stability test of MoS_2 NF membranes*

The stability of M0 and M3 membranes were tested continuously with 2000 ppm Na_2SO_4 at 3.5 bar, the permeation was collected and the salt rejection was measured in every half an hour, the results for both membranes were compared in Fig. 10. It could be found that the MoS_2-TFN membrane exhibited stable permeation of 22.9 L m^{-2} h^{-1} during a long-term operation of 16 h. There existed a flux reduction rate of 6.9%, which was significantly lower than that of pristine TFC membrane

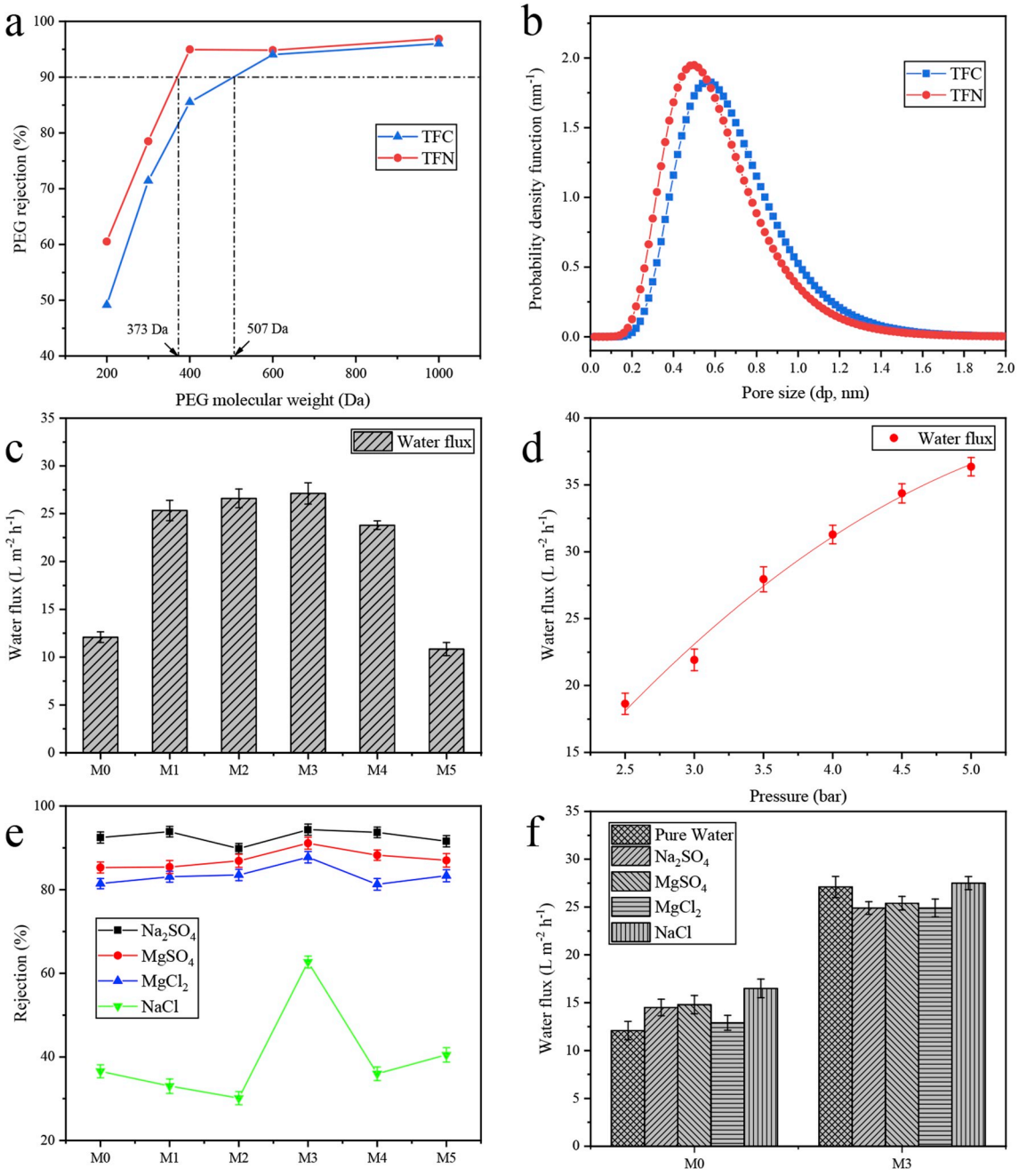

Fig. 9. Molecular weight cut-off (a), pore size and pore size distribution (b) of TFC (M0) and TFN (M3) membranes, pure water flux (c), pressure resistance of M3 (d), salt rejection (e) and water permeation of M0 and M3 (f).

Table 3
Desalination performance of MoS_2-TFN membrane and other MoS_2 membranes.

Membranes	Flux (L m^{-2} h^{-1} bar^{-1})	Na_2SO_4 rejection (%)	Ref.
TFC	3.4	92.5	this work
MoS_2-TFN	7.8	94.4	this work
PDDA@MoS_2	16.5	81.5	[31]
GO@MoS_2	10.2	62.5	[43]
PSBMA@MoS_2	18.1	2.2	[45]

(25.6%). The results showed that the incorporation of MoS_2 could effectively enhance the mechanical stability of the NF membrane. The good stability and the high water desalination capabilities of the MoS_2-TFN membrane demonstrated to be promising in industrial application.

4. Conclusion

Few-layers of 2D MoS_2 were synthesized by a facile solvent-assisted ultrasonic exfoliation method. After TEM and zeta potential characterization, it was found that the size of the prepared MoS_2 after ultrasound was significantly reduced and the electronegativity was enhanced. The MoS_2-TFN membrane was prepared via interfacial polymerization by adding 2D MoS_2 to the organic phase. The effects of incorporating MoS_2 on the morphology, roughness, hydrophilicity, electronegativity and the cross-linking degree of the TFN membrane were characterized. The TFN membrane showed a reduced MWCO and improved desalination performances. The optimal concentration was determined to be 0.010 wt/v %, the flux increased to 27.1 L m^{-2} h^{-1} (7.8 L m^{-2} h^{-1} bar^{-1}), which was 2.3 times than the control with flux of 12.1 L m^{-2} h^{-1} (3.4 L m^{-2} h^{-1} bar^{-1}) without sacrificing the salt rejection. Moreover, it maintained

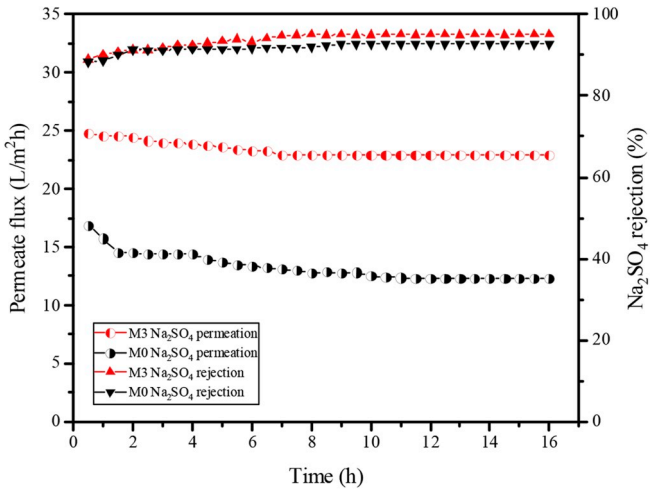

Fig. 10. Stability test of the M0 and M3, 2000 ppm Na_2SO_4 was used as solute.

relative stable during the long-term operation, and was expected to demonstrate its excellent performance in the field of water treatment.

Declaration of competing interest

There are no conflicts to declare.

Acknowledgements

This work was supported by grants from the Bureau of Frontier Sciences and Education (QYZDB-SSW-DQC044), the Bureau of International Cooperation (132C35KYSB20160018), the Chinese Academy of Sciences and the Joint Project between CAS-CSIRO (132C35KYSB20170051). The authors thank the Hongyun Ren and Zhen Xu from Institute of Urban Environment, CAS for the TEM and XPS measurement, respectively. And Danmei Pan from Fujian Institute of Research on the Structure, CAS for the AFM test. Dr. Huali Tian and Dr. Qinliang Jiang, in particular, Dr. Yi Li from the KU Leuven in Belgium gave a lot of advice and help. The authors would like to acknowledge Mrs. Temitope Fausat Ajibade (Nee Otun) for the grammatical revision and reviewers for their valuable comments.

Appendix A. Supplementary data

Supplementary data to this article can be found online at https://doi.org/10.1016/j.memsci.2019.117526.

References

[1] D.M. Warsinger, S. Chakraborty, E.W. Tow, M.H. Plumlee, C. Bellona, S. Loutatidou, L. Karimi, A.M. Mikelonis, A. Achilli, A. Ghassemi, L.P. Padhye, S. A. Snyder, S. Curcio, C. Vecitis, H.A. Arafat, J.H.t. Lienhard, A review of polymeric membranes and processes for potable water reuse, Prog. Polym. Sci. 81 (2016) 209–237.
[2] N. Hilal, H. Al-Zoubi, A.W. Mohammad, N.A. Darwish, Nanofiltration of highly concentrated salt solutions up to seawater salinity, Desalination 184 (2005) 315–326.
[3] Y. Du, Y. Lv, W.Z. Qiu, J. Wu, Z.K. Xu, Nanofiltration membranes with narrowed pore size distribution via pore wall modification, Chem. Commun. 52 (2016) 8589–8592.
[4] S.P. Sun, K.Y. Wang, N. Peng, T.A. Hatton, T.-S. Chung, Novel polyamide-imide/cellulose acetate dual-layer hollow fiber membranes for nanofiltration, J. Membr. Sci. 363 (2010) 232–242.
[5] Y.K. Ong, T.S. Chung, Mitigating the hydraulic compression of nanofiltration hollow fiber membranes through a single-step direct spinning technique, Environ. Sci. Technol. 48 (2014) 13933–13940.
[6] A. Anand, B. Unnikrishnan, J.-Y. Mao, H.-J. Lin, C.-C. Huang, Graphene-based nanofiltration membranes for improving salt rejection, water flux and antifouling–A review, Desalination 429 (2018) 119–133.
[7] P. Marchetti, M.F. Jimenez Solomon, G. Szekely, A.G. Livingston, Molecular separation with organic solvent nanofiltration: a critical review, Chem. Rev. 114 (2014) 10735–10806.
[8] L. Dong, X. Huang, Z. Wang, Z. Yang, X. Wang, C. Tang, A thin-film nanocomposite nanofiltration membrane prepared on a support with in situ embedded zeolite nanoparticles, Separ. Purif. Technol. 166 (2016) 230–239.
[9] B. Rajaeian, A. Rahimpour, M.O. Tade, S. Liu, Fabrication and characterization of polyamide thin film nanocomposite (TFN) nanofiltration membrane impregnated with TiO_2 nanoparticles, Desalination 313 (2013) 176–188.
[10] H. Wu, B. Tang, P. Wu, Optimizing polyamide thin film composite membrane covalently bonded with modified mesoporous silica nanoparticles, J. Membr. Sci. 428 (2013) 341–348.
[11] Y. Li, S. Yang, K. Zhang, B.V.d. Bruggen, Thin film nanocomposite reverse osmosis membrane modified by two dimensional laminar MoS_2 with improved desalination performance and fouling-resistant characteristics, Desalination 454 (2019) 48–58.
[12] S. Abdikheibari, W. Lei, L.F. Dumée, A.J. Barlow, K. Baskaran, Novel thin film nanocomposite membranes decorated with few-layered boron nitride nanosheets for simultaneously enhanced water flux and organic fouling resistance, Appl. Surf. Sci. 488 (2019) 565–577.
[13] X. Wu, R.W. Field, J.J. Wu, K. Zhang, Polyvinylpyrrolidone modified graphene oxide as a modifier for thin film composite forward osmosis membranes, J. Membr. Sci. 540 (2017) 251–260.
[14] G.-R. Xu, J.-M. Xu, H.-C. Su, X.-Y. Liu, L. Lu, H.-L. Zhao, H.-J. Feng, R. Das, Two-dimensional (2D) nanoporous membranes with sub-nanopores in reverse osmosis desalination: latest developments and future directions, Desalination 451 (2019) 18–34.
[15] Q. Liu, G.-R. Xu, Graphene oxide (GO) as functional material in tailoring polyamide thin film composite (PA-TFC) reverse osmosis (RO) membranes, Desalination 394 (2016) 162–175.
[16] Y. Yuan, X. Gao, Y. Wei, X. Wang, J. Wang, Y. Zhang, C. Gao, Enhanced desalination performance of carboxyl functionalized graphene oxide nanofiltration membranes, Desalination 405 (2017) 29–39.
[17] S. Kim, X. Lin, R. Ou, H. Liu, X. Zhang, G.P. Simon, C.D. Eastonc, H. Wang, Highly crosslinked, chlorine tolerant polymer network entwined graphene oxide membrane for water desalination, J. Mater. Chem. 5 (2017) 1533–1540.
[18] M.-Y. Lim, Y.-S. Choi, J. Kim, K. Kim, H. Shin, J.-J. Kim, D.M. Shin, J.-C. Lee, Cross-linked graphene oxide membrane having high ion selectivity and antibacterial activity prepared using tannic acid-functionalized graphene oxide and polyethyleneimine, J. Membr. Sci. 521 (2017) 1–9.
[19] K. Goh, L. Setiawan, L. Wei, R. Si, A.G. Fane, R. Wang, Y. Chen, Graphene oxide as effective selective barriers on a hollow fiber membrane for water treatment process, J. Membr. Sci. 474 (2015) 244–253.
[20] M. Hu, B. Mi, Enabling graphene oxide nanosheets as water separation membranes, Environ. Sci. Technol. 47 (2013) 3715–3723.
[21] S. Bano, Asif Mahmood, S. Kima, K. Lee, Graphene oxide modified polyamide nanofiltration membrane with improved flux and antifouling properties, J. Mater. Chem. 3 (2015) 2065–2071.
[22] C. Yeh, K. Raidongia, J. Shao, Q. Yang, J. Huang, On the origin of the stability of graphene oxide membranes in water, Nat. Chem. 7 (2015) 166–170.
[23] P. Zhang, J.-L. Gong, G.-M. Zeng, C.-H. Deng, H.-C. Yang, H.-Y. Liu, S.-Y. Huan, Cross-linking to prepare composite graphene oxide-framework membranes with high-flux for dyes and heavy metal ions removal, Chem. Eng. J. 322 (2017) 657–666.
[24] J.H. Jang, J.Y. Woo, J. Lee, C.S. Han, Ambivalent effect of thermal reduction in mass rejection through graphene oxide membrane, Environ. Sci. Technol. 50 (2016) 10024–10030.
[25] H. Gao, Q. Shi, D. Rao, Y. Zhang, J. Su, Y. Liu, Y. Wang, K. Deng, R. Lu, Rational design and strain engineering of nanoporous boron nitride nanosheet membranes for water desalination, J. Phys. Chem. C 121 (2017) 22105–22113.
[26] J. Azamat, Removal of nickel (II) from aqueous solution by graphene and boron nitride nanosheets, J. Water Environ. Nanotechnol. 2 (2017) 26–33.
[27] S. Abdikheibari, W. Lei, L.F. Dumée, N. Milnea, K. Baskarana, Thin film nanocomposite nanofiltration membranes from amine functionalized-boron nitride/polypiperazine amide with enhanced flux and fouling resistance, J. Mater. Chem. 6 (2018) 12066–12081.
[28] W. Lei, V.N. Mochalin, D. Liu, S. Qin, Y. Gogotsi, Y. Chen, Boron nitride colloidal solutions, ultralight aerogels and freestanding membranes through one-step exfoliation and functionalization, Nat. Commun. 6 (2015), 8849.
[29] C. Chen, J. Wang, D. Liu, C. Yang, Y. Liu, R.S. Ruoff, W. Lei, Functionalized boron nitride membranes with ultrafast solvent transport performance for molecular separation, Nat. Commun. 9 (2018), 1902.
[30] Z.-X. Low, J. Ji, D. Blumenstock, Y.-M. Chew, D. Wolverson, D. Mattia, Fouling resistant 2D boron nitride nanosheet – PES nanofiltration membranes, J. Membr. Sci. 563 (2018) 949–956.
[31] J. Zhou, Z. Qin, Y. Lu, X. Li, Q. An, S. Ji, N. Wang, H. Guo, MoS_2/polyelectrolytes hybrid nanofiltration (NF) membranes with enhanced permselectivity, J. Taiwan Inst. Chem. Eng. 84 (2018) 196–202.
[32] M.S.S.A. Saraswathi, D. Rana, P. Vijayakumar, S. Alwarappan, A. Nagendran, Tailored PVDF nanocomposite membranes using exfoliated MoS_2 nanosheets for improved permeation and antifouling performance, New J. Chem. 41 (2017) 14315–14324.
[33] W. Li, Y. Yang, J.K. Weber, G. Zhang, R. Zhou, Tunable, strain-controlled nanoporous MoS_2 filter for water desalination, ACS Nano 10 (2016) 1829–1835.
[34] W. Choi, N. Choudhary, G.H. Han, J. Park, D. Akinwande, Y.H. Lee, Recent development of two-dimensional transition metal dichalcogenides and their applications, Mater. Today 20 (2017) 116–130.

[35] J. Azamat, A. Khataee, F. Sadikoglu, Computational study on the efficiency of MoS_2 membrane for removing arsenic from contaminated water, J. Mol. Liq. 249 (2018) 110–116.
[36] Z. Wang, B. Mi, Environmental applications of 2D molybdenum disulfide (MoS_2) nanosheets, Environ. Sci. Technol. 51 (2017) 8229–8244.
[37] Z. Wang, Q. Tu, S. Zheng, J.J. Urban, S. Li, B. Mi, Understanding the aqueous stability and filtration capability of MoS_2 membranes, Nano Lett. 17 (2017) 7289–7298.
[38] D. Wang, Z. Wang, L. Wang, L. Hu, J. Jin, Ultrathin membranes of single-layered MoS_2 nanosheets for high-permeance hydrogen separation, Nanoscale 7 (2015) 17649–17652.
[39] F. Pan, H. Ding, W. Li, Y. Song, H. Yang, H. Wu, Z. Jiang, B. Wang, X. Cao, Constructing facilitated transport pathway in hybrid membranes by incorporating MoS_2 nanosheets, J. Membr. Sci. 545 (2018) 29–37.
[40] M. Heiranian, A.B. Farimani, N.R. Aluru, Water desalination with a single-layer MoS_2 nanopore, Nat. Commun. 6 (2015), 8616.
[41] L. Sun, H. Huang, X. Peng, Laminar MoS_2 membranes for molecule separation, Chem. Commun. 49 (2013) 10718–10720.
[42] J. Azamat, A. Khataee, Improving the performance of heavy metal separation from water using MoS_2 membrane: molecular dynamics simulation, Comput. Mater. Sci. 137 (2017) 201–207.
[43] P. Zhang, J.-L. Gong, G.-M. Zeng, B. Song, W. Cao, H.-Y. Liu, S.-Y. Huan, P. Peng, Novel "loose" GO/MoS_2 composites membranes with enhanced permeability for effective salts and dyes rejection at low pressure, J. Membr. Sci. 574 (2019) 112–123.
[44] J. Gao, M. Zhang, J. Wang, G. Liu, H. Liu, Y. Jiang, Bioinspired modification of layer-stacked molybdenum disulfide (MoS_2) membranes for enhanced nanofiltration performance, ACS Omega 4 (2019) 4012–4022.
[45] X. Liang, P. Wang, J. Wang, Y. Zhang, W. Wu, J. Liu, B. Van der Bruggen, Zwitterionic functionalized MoS_2 nanosheets for a novel composite membrane with effective salt/dye separation performance, J. Membr. Sci. 573 (2019) 270–279.
[46] J.N. Coleman, M. Lotya, A. O'Neill, Two-dimensional nanosheets produced by liquid exfoliation of layered materials, Science 331 (2011) 568–571.
[47] X. Huang, Z. Zeng, H. Zhang, Metal dichalcogenide nanosheets: preparation, properties and applications, Chem. Soc. Rev. 42 (2013) 1934–1946.
[48] Y. Hernandez, V. Nicolosi, M. Lotya, F.M. Blighe, Z. Sun, S. De, I.T. McGovern, B. Holland, M. Byrne, Y.K. Gun'Ko, J.J. Boland, P. Niraj, G. Duesberg, S. Krishnamurthy, R. Goodhue, J. Hutchison, V. Scardaci, A.C. Ferrari, J. N. Coleman, High-yield production of graphene by liquid-phase exfoliation of graphite, Nat. Nanotechnol. 3 (2008) 563–568.
[49] H. Ma, Z. Shen, S. Ben, Understanding the exfoliation and dispersion of MoS_2 nanosheets in pure water, J. Colloid Interface Sci. 517 (2018) 204–212.
[50] R. Pang, K. Zhang, Fabrication of hydrophobic fluorinated silica-polyamide thin film nanocomposite reverse osmosis membranes with dramatically improved salt rejection, J. Colloid Interface Sci. 510 (2018) 127–132.
[51] S. Karan, Z. Jiang, A.G. Livingston, Sub-10 nm polyamide nanofilms with ultrafast solvent transport for molecular separation, Science 348 (2015) 1347–1351.
[52] Y. Li, E. Wong, Z. Mai, B. Van der Bruggen, Fabrication of composite polyamide/Kevlar aramid nanofiber nanofiltration membranes with high permselectivity in water desalination, J. Membr. Sci. 592 (2019), 117396.
[53] Y. Li, E. Wong, A. Volodine, C.V. Haesendonck, K. Zhang, B.V.d. Bruggen, Nanofibrous hydrogel composite membranes with ultrafast transport performance for molecular separation in organic solvents, J. Mater. Chem. A 7 (2019) 19269–19279.
[54] T.H. Lee, J.Y. Oh, S.P. Hong, J.M. Lee, S.M. Roh, S.H. Kim, H.B. Park, ZIF-8 particle size effects on reverse osmosis performance of polyamide thin-film nanocomposite membranes: importance of particle deposition, J. Membr. Sci. 570–571 (2019) 23–33.
[55] H. Dong, L. Wu, L. Zhang, H. Chen, C. Gao, Clay nanosheets as charged filler materials for high-performance and fouling-resistant thin film nanocomposite membranes, J. Membr. Sci. 494 (2015) 92–103.
[56] H. Dong, L. Zhao, L. Zhang, H. Chen, C. Gao, W.S. Winston Ho, High-flux reverse osmosis membranes incorporated with NaY zeolite nanoparticles for brackish water desalination, J. Membr. Sci. 476 (2015) 373–383.
[57] S.-M. Xue, C.-H. Ji, Z.-L. Xu, Y.-J. Tang, R.-H. Li, Chlorine resistant TFN nanofiltration membrane incorporated with octadecylamine-grafted GO and fluorine-containing monomer, J. Membr. Sci. 545 (2018) 185–195.
[58] B. Radisavljevic, A. Radenovic, J. Brivio, V. Giacometti, A. Kis, Single-layer MoS_2 transistors, Nat. Nanotechnol. 6 (2011) 147–150.
[59] J. Kibsgaard, Z. Chen, B.N. Reinecke, T.F. Jaramillo, Engineering the surface structure of MoS_2 to preferentially expose active edge sites for electrocatalysis, Nat. Mater. 11 (2012) 963–969.
[60] Q. Xia, Q. Tan, Tubular hierarchical structure composed of O-doped ultrathin MoS_2 nanosheets grown on carbon microtubes with enhanced lithium ion storage properties, J. Alloy. Comp. 779 (2019) 156–166.
[61] Z. Tan, S. Chen, X. Peng, L. Zhang, C. Gao, Polyamide membranes with nanoscale Turing structures for water purification, Science 360 (2018) 518–521.
[62] M. Amini, S.A.A. Ramazani, M. Faghihi, S. Fattahpour, Preparation of nanostructured and nanosheets of MoS_2 oxide using oxidation method, Ultrason. Sonochem. 39 (2017) 188–196.
[63] G.N.B. Baroña, J. Lim, M. Choi, B. Jung, Interfacial polymerization of polyamide-aluminosilicate SWNT nanocomposite membranes for reverse osmosis, Desalination 325 (2013) 138–147.
[64] L.M. Jin, S.L. Yu, W.X. Shi, X.S. Yi, N. Sun, Y.L. Ge, C. Ma, Synthesis of a novel composite nanofiltration membrane incorporated SiO_2 nanoparticles for oily wastewater desalination, Polymer 53 (2012) 5295–5303.
[65] H.-R. Chae, J. Lee, C.-H. Lee, I.-C. Kim, P.-K. Park, Graphene oxide-embedded thin-film composite reverse osmosis membrane with high flux, anti-biofouling, and chlorine resistance, J. Membr. Sci. 483 (2015) 128–135.
[66] B. Tansel, J. Sager, T. Rector, J. Garland, R.F. Strayer, L. Levine, M. Roberts, M. Hummerick, J. Bauer, Significance of hydrated radius and hydration shells on ionic permeability during nanofiltration in dead end and cross flow modes, Separ. Purif. Technol. 51 (2006) 40–47.
[67] L. Yuwen, Y. Sun, G. Tan, W. Xiu, Y. Zhang, L. Weng, Z. Teng, L. Wang, MoS_2@polydopamine-Ag nanosheets with enhanced antibacterial activity for effective treatment of Staphylococcus aureus biofilms and wound infection, Nanoscale 10 (2018) 16711–16720.
[68] J. Wang, H. Yang, M. Wu, X. Zhang, Z. Xu, Nanofiltration membranes with cellulose nanocrystals as an interlayer for unprecedented performance, J. Mater. Chem. 5 (2017) 16289–16295.
[69] Z. Wang, Z. Wang, S. Lin, H. Jin, S. Gao, Y. Zhu, J. Jin, Nanoparticle-templated nanofiltration membranes for ultrahigh performance desalination, Nat. Commun. 9 (2018), 2004.
[70] L. Bai, Y. Liu, A. Ding, N. Ren, G. Li, H. Liang, Fabrication and characterization of thin-film composite (TFC) nanofiltration membranes incorporated with cellulose nanocrystals (CNCs) for enhanced desalination performance and dye removal, Chem. Eng. J. 358 (2019) 1519–1528.
[71] C.Y. Tang, Y.-N. Kwon, J.O. Leckie, Effect of membrane chemistry and coating layer on physiochemical properties of thin film composite polyamide RO and NF membranes I. FTIR and XPS characterization of polyamide and coating layer chemistry, Desalination 242 (2009) 149–167.